HOKKAIDO UNIVERSITY

Title	Rapid physically driven inversion of the air-sea ice CO2 flux in the seasonal landfast ice off Barrow, Alaska after onset of surface melt
Author(s)	Nomura, Daiki; Eicken, Hajo; Gradinger, Rolf et al.
Citation	Continental Shelf Research, 30(19), 1998-2004 https://doi.org/10.1016/j.csr.2010.09.014
Issue Date	2010-11-30
Doc URL	https://hdl.handle.net/2115/44792
Type	journal article
File Information	CSR30-19_1998-2004.pdf

Hokkaido University Collection of Scholarly and Academic Papers : HUSCAP

Rapid physically driven inversion of the air–sea ice CO_2 flux in the seasonal landfast ice off Barrow, Alaska after onset of surface melt

Daiki Nomura[a, b, c], Hajo Eicken[d], Rolf Gradinger[e] and Kunio Shirasawa[b]

[a] *National Institute of Polar Research, 10-3 Midori-cho, Tachikawa, Tokyo 190-8518, Japan*

[b] *Institute of Low Temperature Science, Hokkaido University, Kita-19, Nishi-8, Kita-ku, Sapporo 060-0819, Japan*

[c] *Graduate School of Environmental Science and Faculty of Environmental Earth Science, Hokkaido University, Kita-10, Nishi-5, Kita-ku, Sapporo 060-0810, Japan*

[d] *Geophysical Institute, University of Alaska Fairbanks, P.O. Box 757320, Fairbanks, AK 99775-7320, USA*

[e] *School of Fisheries and Ocean Sciences, University of Alaska Fairbanks, P.O. Box 757220, Fairbanks, AK 99775-7220, USA*

Received 25 September 2009; revised 16 July 2010; accepted 28 September 2010. Available online 7 October 2010.

Abstract

The air–sea ice CO_2 flux was measured over landfast sea ice in the Chukchi Sea, off Barrow, Alaska in late May 2008 with a chamber technique. The ice cover transitioned from a cold early spring to a warm late spring state, with an increase in air temperature and incipient surface melt. During melt, brine salinity and brine dissolved inorganic carbon concentration (DIC) decreased from 67.3 to 18.7 and 3977.6 to 1163.5 μ mol kg $^{-1}$, respectively. In contrast, the salinity and DIC of under-ice water at depths of 3 and

5 m below the ice surface remained almost constant with average values of 32.4±0.3 (standard deviation) and 2163.1±16.8 μ mol kg^{-1}, respectively. The air–sea ice CO_2 flux decreased from +0.7 to −1.0 mmol m^{-2} day^{-1} (where a positive value indicates CO_2 being released to the atmosphere from the ice surface). During this early to late spring transition, brought on by surface melt, sea ice shifted from a source to a sink for atmospheric CO_2, with a rapid decrease of brine DIC likely associated with a decrease in the partial pressure of CO_2 of brine from a supersaturated to an undersaturated state compared to the atmosphere. Formation of superimposed ice coincident with melt was not sufficient to shut down ice–air gas exchange.

Keywords: Sea ice; Brine; CO_2 flux; pCO_2; Chukchi sea; Arctic ocean

1. Introduction

Measurements of the partial pressure of CO_2 (pCO_2) in surface waters are an important prerequisite to evaluate the air–sea CO_2 flux in the world's oceans. Only limited data are available for high latitude regions, particularly during winter, when the oceans are covered by sea ice (e.g., Takahashi et al., 2009). As underlined by Tison et al. (2002), it is often assumed that sea ice effectively caps the surface ocean, greatly restricting gas exchange between the ocean and atmosphere. However, recent observations question this paradigm and suggest that sea ice is a permeable medium for CO_2, at least part of the year ([Semiletov et al., 2004], [Semiletov et al., 2007], [Delille, 2006], [Nomura et al., 2006], [Nomura et al., in press-a] and [Zemmelink et al., 2006]).

This work is motivated by past studies of CO_2 exchange in the Chukchi Sea, a marginal shelf sea of the Arctic Ocean, with its western limit defined by Wrangel Island and Point Barrow bordering on the eastern margin. Extremely low pCO_2 have been observed in ice-free Chukchi Sea surface waters in late spring through an early autumn, corresponding to high primary productivity and indicating that the waters represent a significant CO_2 sink for the atmosphere ([Pipko et al., 2002] and

2007]). In the eastern Chukchi Sea up to Point Barrow, landfast ice occurs in the nearshore region from typically November through June ([Mahoney et al., 2007] and [Druckenmiller et al., 2009]). During spring melt in June, sea–ice melt ponds and brine channels in the ice cover represent an important sink for atmospheric CO_2 (Semiletov et al., 2004). Earlier in the season during the ice-growth period (February), under-ice water pCO_2 is supersaturated with respect to the atmosphere as detected by moored CO_2 sensors ([Semiletov et al., 2004] and [Semiletov et al., 2007]). Brines also experience pCO_2 supersaturation with decreasing ice temperatures and increasing brine salinities during the first part of the ice-growth season (e.g., Papadimitriou et al., 2003). Thus, CO_2 can be emitted from brine channels to the underlying water and – if the ice permeability is sufficiently high – to the overlying atmosphere ([Nomura et al., 2006], [Nomura et al., in press-a], [Rysgaard et al., 2007] and [Loose et al., 2009]). These processes complicate the net annual balance between the uptake and outgassing through Arctic sea ice (Semiletov et al., 2007), requiring detailed observational data to gain further insight into the timing and physical controls of the cold/warm transition between sea ice as a seasonal source and sink of CO_2. Such data are also necessary to improve assessments and modeling of regional and seasonal carbon budgets in the Arctic.

We studied the air–sea ice CO_2 flux during the ice cover's transition from a cold early spring to a warm late spring state in the Chukchi Sea, off Barrow, Alaska in late May 2008. The aim of the present study was to examine variability in the air–sea ice CO_2 flux during changing surface states of the ice cover in conjunction with variability in the atmospheric variables, such as air temperature and changes in the properties of surface snow, brine and sea ice.

2. Measurements and sampling methods

Field observations were carried out 19–26 May 2008 on landfast first-year sea ice in the Chukchi Sea, off Barrow, Alaska (Fig. 1). The temporal variations of the air–sea ice CO_2 flux and the physico-chemical properties of brine and under-ice water were examined at a fixed sampling station (71°19′ 51.5″ N, 156°41′ 17.4″ W) located

approximately 1 km offshore at a water depth of approximately 6 m. Each observation was carried out from morning (9:00a.m.) to afternoon (13:00p.m.).

Measurements of air and sea ice temperatures were available from the Barrow sea ice mass balance site near our sampling location for the period February through June 2008 (http://seaice.alaska.edu/gi/data/barrow_massbalance; Druckenmiller et al. 2009). Briefly, the air temperature was measured at a height of 2 m above the ice surface with a shielded Campbell CS500 sensor. Vertical temperature profiles within the sea ice were measured at 10 cm intervals with thermistor strings and recorded with Campbell CS500 logger.

The air–sea ice CO_2 flux was measured with a closed chamber approach, allowing direct determination of the *in situ* CO_2 flux over sea ice (Nomura et al., in press-a). Replicate measurements for CO_2 flux were carried out on 20, 22 and 23 May 2008 within the same time frame (2–3 h) and area (within 1 m^2) as the other measurements. A stainless steel chamber with no fan (50 cm in diameter and 30 cm in height with the serrated bottom edge) was positioned directly over the snow at the sampling site. The chamber was then pushed down firmly into the snow and sea ice to prevent lateral diffusion of CO_2. The air sampled from within the chamber passed through Teflon tubes connected to a non-dispersive infrared (NDIR) analyzer (carbon dioxide probe, GMP343, Vaisala, Finland) which was connected to a data logger (RVR 52, T & D Corp., Japan). Temperatures in the chamber were measured during each flux measurement, using a temperature data logger (RTR 52, T & D Corp., Japan). The air in the chamber was circulated with a pump at a flow rate of 0.7 L min^{-1} through a mass flow controller and chemical desiccant column containing $Mg(ClO_4)_2$. These devices were installed in a portable adiabatic box (40×25×30 cm^3). Electricity was provided by a portable electric generator. The CO_2 concentration in the chamber was measured every 10 s for each experiment's total duration of 40 min. Four standards (mixing ratio of 324, 341, 363 and 406 ppm) traceable to the World Meteorological Organization (WMO) mole fraction scale (Inoue and Ishii, 2005) were used to calibrate the CO_2 measuring system prior to an *in situ* observation. The air–sea ice CO_2 flux was calculated according to

$F = \rho (273.15/T)(dC/dt)(V/A)$ (1)

where F is the flux (mmol C m^{-2} day^{-1}), ρ is the CO_2 density at standard temperature and pressure (=44.5 mol m^{-3}×(12/44)), T is the temperature in the chamber (°K), dC/dt is the rate of time variation (ppm day^{-1}) of CO_2 concentration in chamber, V is the volume (m^3) of the chamber headspace adjusted for the volume occupied by the solid phase of snow and A the sea ice surface area (m^2) sampled by the chamber. The values of 12 and 44 indicate the atomic mass of carbon and molecular mass of CO_2, respectively. The ratio of 273.15/T corrects for the temperature effect relative to the standard state. The stability of our NDIR has been verified during CO_2 concentration measurements. Hence, r^2 for the model from which fluxes have been derived scaled with the magnitude of dC/dtin Eq. (1) (Mariko et al., 1994). The precision of the air–sea ice CO_2 flux examined by duplicate measurements (n=14) was within ±0.2 mmol m^{-2} day^{-1} (Nomura et al., in press-a). The detection limit of the CO_2 flux was <0.1 mmol m^{-2} day^{-1}, which was estimated from the precision of the NDIR. The accuracy of the air–sea ice CO_2 flux is difficult to establish, because the true value of CO_2 flux between sea ice and the atmosphere could not be quantified. The CO_2 flux estimated by chamber methods can be affected by many factors which are not easy to evaluate. For example, the CO_2 flux is influenced by wind-driven variations in atmospheric pressure ([Winston et al., 1995], [Luo and Zhou, 2006] and [Takagi et al., 2005]). Additionally, air in the chamber has to be mixed without generating localized pressure gradients (Luo and Zhou, 2006). Furthermore, the buffering effect of the snow can allow CO_2 to build up in the snowpack in the case of outgassing ([Takagi et al., 2005] and [Zemmelink et al., 2006]). When the flux chamber is placed over the snow, this excess CO_2 may be released into the chamber, particularly if a fan is used. In order to overcome these restrictions, we adjusted the gas flow with a pump (rather than a fan) to homogenize the sample air within the chamber. The mass flow controller that regulates pressure was carefully adjusted to minimize the pressure differential between the inside and outside of the chamber. Also, during the measurement period, the wind speeds were low with a mean of 3.4 m s^{-1}, suggesting that the wind-driven turbulent flux was small, reducing impacts on derived CO_2 fluxes. Other factors influencing the

CO_2 flux are that the changes of CO_2 concentration in the chamber can suppress the real CO_2 flux with respect to the ambient CO_2 concentration (Winston et al., 1995). We used a chamber with a large volume to minimize the impact of temporal variations in the CO_2 concentration (Nomura et al., in press-b). Therefore, the data collected with our chamber system should be close to the true flux values during the observation period.

Our chamber system was very similar to other systems generally employed for measurements over sea ice (Delille, 2006), snow (Winston et al., 1995; Schindlbacher et al., 2007) and the ocean (Frankignoulle, 1998). Therefore, we argue that our results can be directly compared against other chamber measurements. For example, as shown in Nomura et al. (in press-a), we were able to compare our data with those of Delille (2006). Briefly, when the brine pCO_2 was of the same order of magnitude, the range of CO_2 flux values obtained from the chamber method was identical between our measurements and Delille's study.

Sea ice was collected using an ice corer with an inner diameter of 9 cm (Mark II coring system, Kovacs Enterprises, Inc., USA). Ice temperatures were measured by inserting a needle-type temperature sensor (Fisher-Scientific Traceable Datalog Digital Thermometer, Thermo Fisher Scientific Inc., USA) in the holes drilled into the core immediately after the sample was collected. Then, the ice core was cut with a stainless steel saw and ice sections were placed into new polyethylene zip-lock bags. Thereafter, the ice samples were transported to the Ukpeaġvik Iñupiat Corporation (UIC)-Naval Arctic Research Laboratory (NARL) (Fig. 1).

Brine samples from sea ice were obtained using the sack hole method (e.g., Gleitz et al., 1995). A 0.5 m depth hole was drilled below the ice surface using an ice corer, and then covered with a 5 cm-thick urethane lid to reduce heat and gas transfer across the brine/atmosphere interface. After the brine accumulated at the bottom of the hole over a period of approximately 10–15 min, the brine was sampled with a polypropylene syringe. The collected brine sample was split between two vials: a 10-mL plastic vial for measuring salinity and a 120-mL glass vial for measuring the dissolved inorganic carbon (DIC) of the brine. An amount of 50-μL saturated-mercuric chloride ($HgCl_2$)

was added to the DIC sample to terminate biological activity. The total alkalinity (TA) of the brine was not measured, since the volume of the collected brine was insufficient. Temperatures of the brine were measured by inserting a needle-type temperature sensor into the volume of brine filling up the hole.

Under-ice water was collected approximately 15 min after drilling a hole in order to avoid any disturbances caused by drilling (Nomura et al., 2009). A Kemmerer water sampler was used to collect under-ice water through the hole in sea ice at depths of 3 and 5 m below the sea–ice surface. Temperatures of the under-ice water were measured by inserting a needle-type temperature sensor into the outlet of the sampling tube connected to the water sampler. The water samples were treated in the same manner as the brine samples for further analysis. The amount of water was large enough to measure both DIC and TA.

3. Sample analysis

The salinity of the melted ice was measured with an YSI Oxygen, Conductivity, Salinity and Temperature reader (YSI 85, YSI Inc., USA) at NARL, while the salinity of the brine and the under-ice water samples were measured, using a salt analyzer (SAT-210, Toa Electronics Ltd., Japan) at Hokkaido University, Sapporo (Nomura et al., 2006). Stable-isotope ($\delta\ ^{18}O$) measurements were carried out at the Stable Isotope Ratio Facility for Environmental Research at the University of Utah. Stable-isotope measurements were performed on a Finnigan Delta V mass spectrometer (carbon dioxide equilibration, measured against VSMOW).

Analysis of DIC in the brine and under-ice water was through coulometry (Johnson et al., 1985), calibrated with working seawater standards traceable to the Certified Reference Material distributed by Prof. A. G. Dickson (Scripps Institution of Oceanography, La Jolla, California, USA). The precision of DIC analysis from duplicate determination was within ±0.1% (

The TA of under-ice water was measured with a glass electrode calibrated with Tris buffer and 2-aminopyridine buffer (DOE, 1994), and then analyzed by the improved single point titration method (Culberson et al., 1970). The precision of TA analysis from duplicate determination was within ±0.2% (Wakita et al., 2005).

The pCO_2 of under-ice water was computed from DIC and TA with the computer program CO2SYS (Lewis and Wallace, 1998). We used the carbonate dissociation constants (K_1 and K_2) after Mehrbach et al. (1973) as refit by Dickson and Millero (1987), and the KSO_4 determined by Dickson (1990). These constants were given as a function of temperature from 0 to 45 °C and salinity from 5 to 45 (e.g., [DOE, 1994] and [Millero, 1995]). Here, we use the equilibrium constants outside their reported range of applicability, assuming that the same functional relationships hold for low-temperature and high-salinity sea ice, following previous studies ([Delille, 2006], [Nomura et al., 2006] and [Thomas et al., 2010]).

Overlying air CO_2, concentration was measured for 20 min prior to the measurement of air–sea ice CO_2 flux. During this period, the chamber was left open to the atmosphere. The air pCO_2 was calculated from the overlying air CO_2 concentration by assuming a barometric pressure of 1 atm and saturated water vapor of the brine (Weiss and Price, 1980).

Chlorophyll *a in vivo* fluorescence of under-ice and ice meltwater was determined using a WATER-PAM fluorometer (Walz Mass-und Regeltechnik, Germany), chlorophyll *a* concentrations were then calculated on the basis of a conversion factor, that was established by extracting five samples from one of the sampling site in 90% acetone and the chlorophyll *a* determination according to Arar and Collins (1992).

The brine volume of sea ice was calculated from the temperature and bulk salinity of sea ice according to Cox and Weeks (1983) for temperatures below −2 °C, and according to Leppäranta and Manninen (1988) for temperatures within the range 0 to −2 °C.

4. Results

4.1. Air and sea ice temperature at the Barrow sea ice mass balance site

A sharp increase in air temperature was observed from 13 to 16 May, just prior to the sampling period; the air temperature began to exceed 0.0 °C on 20 May (Fig. 2a). Ice temperatures varied – though delayed by thermal conduction – with air temperature and increased rapidly to −1.0 °C at the surface of sea ice at the end of our sampling period on 26 May (Fig. 2b). Rapid surface warming was also promoted by rain events that lasted a few hours, starting on 24 May. Rain and snow meltwater percolated down to the ice–snow interface and resulted in the formation of superimposed ice, typically several centimeters in thickness.

4.2. Sea ice thickness and snow depth

Sea ice thickness was almost constant in the range 144–157 cm with an average of 149±5 cm (standard deviation) during the sampling period (Fig. 3a). There was a considerable decrease in the snow depth from 16 cm on 20 May to only 2 cm on 26 May, due to snow melting caused by the increase in air temperature, rain events and high fluxes of solar radiation (Figs. 2 and 3b). Superimposed ice of roughly 3 cm thickness was observed at the base of the snowpack (visible in the core stratigraphy photograph shown in Fig. 4b), but no presence of a slush layer could be detected.

4.3. Sea ice bulk salinity, temperature, brine volume, chlorophyll *a* concentration and $\delta^{18}O$

Salinity profiles exhibit a weakly defined C-shape, decreasing from approximately 7–3

across 15 and 140 cm depth, then increasing to between 8 and 14 at the ice base (Fig. 5a). Values ranged1–7 at the surface. As observed at the sea ice mass balance site (in Fig. 2b), the increase in ice temperature was prominent in the upper ice layer compared to the middle and bottom (Fig. 5b). The brine volume was higher than 5% throughout the ice core (Fig. 5c), indicating that dissolved constituents like CO_2 in the brine were capable of diffusing through the brine channel network, due to higher permeability of sea ice (Golden et al., 1998). Chlorophyll *a* concentrations ranged152–322 μ g l^{-1} in the bottom layer of the ice, while they were negligible everywhere else (Fig. 5d).

As shown in Fig. 4, a 3 cm-thick layer of relatively clear, low-salinity ice with $\delta^{18}O$ of −11.8‰ was found above the whitish granular and darker columnar ice in the uppermost ice layers. With $\delta^{18}O$ for snow ranging between −19.8 and −23.2‰, this layer was composed to more than half of the meteoric water, indicative of superimposed ice forming as a result of snow melt and rain refreezing on top of the cold sea ice in the early melt season.

4.4. Physico-chemical properties of brine and under-ice water

Brine temperatures increased from −3.7 °C on 19 May to −2.3 °C on 26 May, while temperatures of under-ice water were constant at −1.7±0.0 °C during the sampling period (Fig. 6a). Brine salinity decreased drastically from 67.3 on 19 May to 18.7 on 26 May, while the salinity of under-ice water was constant at 32.4±0.3 (Fig. 6b).

In accordance with the temporal variations of brine and under-ice water in salinity (Fig. 6b), the DIC of brine decreased from 3977.6 μ mol kg^{-1} on 19 May to 1163.5 μ mol kg^{-1} on 26 May, while the DIC of under-ice water remained constant at 2163.1±16.8 μ mol kg^{-1} (Fig. 6c).

In order to assess the effects of dilution and/or concentration processes on the DIC in the brine, as opposed to the carbon uptake and/or release by biological activity, data were normalized to a salinity of 32.4, the mean value of under-ice water salinity during the sampling period (Fig. 6b, c and d). The normalized-brine DIC was constant throughout the sampling period (Fig. 6d). In addition, the salinity and DIC of brine and under-ice water are highly correlated (r^2=0.99, p<0.001; not shown). These results indicate that the decrease of brine DIC was mainly caused by dilution, due to melting of snow and ice rather than biological uptake by photosynthesis. TA of under-ice water was constant at 2247.3±8.0 μ mol kg^{-1} during the sampling period. Chlorophyll *a* concentration of under-ice water ranged 0.1–2.3 μ g l^{-1} with a mean of 1.0 μ g l^{-1} during the sampling period.

The pCO_2 for under-ice water was almost constant at 424.8±18.8 μ atm and was slightly higher than that for the atmosphere (395.5±3.5 μ atm) throughout the sampling period.

4.5. Temporal variations of the air–sea ice CO_2 flux

The air–sea ice CO_2 flux was positive in the range between +0.1 and +0.7 mmol m^{-2} day^{-1} from 19 to 23 May, while it was negative at −1.0 mmol m^{-2} day^{-1} on 26 May (Fig. 7). This illustrates that the sea ice cover switched from a CO_2 source to a CO_2 sink during the observation period.

5. Discussion

The air–sea ice CO_2 flux underwent a change from positive (+0.7 mmol m^{-2} day^{-1}) to negative (−1.0 mmol m^{-2} day^{-1}) during the sampling period, tracking the variations of brine salinity and brine DIC (Fig. 6). The constant normalized-brine DIC throughout the sampling period (Fig. 6d) indicates that brine DIC was mainly controlled by the influx

meltwater almost devoid of DIC, at least in the ice interior, where ice temperatures and incipient salinity reductions were evident in bulk salinity and brine salinity ([Fig. 5] and [Fig. 6]).

Brine pCO_2 is an important factor controlling the air–sea ice CO_2 flux (e.g., Nomura et al., 2006). Although we did not estimate brine pCO_2, the variations of brine DIC and brine salinity can help to understand pCO_2 dynamics. Previous studies indicated that brine pCO_2 changes dramatically from the season of sea ice formation to melting conditions ([Papadimitriou et al., 2003], [Delille, 2006] and [Nomura et al., 2006]). During sea ice formation, brine pCO_2 increases with increases in brine DIC, and with changes in CO_2 solubility and the dissociation constants of carbonic acid as a function of brine salinity, which increases as a result of the progressive rejection of dissolved impurities from growing ice (Nomura et al., 2006). Therefore, brine pCO_2 is supersaturated with respect to the air during periods of ice growth. On the other hand, during ice melt, the same process occurs for brine pCO_2 due to the dilution effect, but in the opposite direction (decrease in brine pCO_2 with decreases in brine DIC). This explains the observed transition of the air–sea ice CO_2 flux from positive to negative as a consequence of reducing pCO_2 during the period of ice melt. The biological productivity in sea ice also reduces the brine pCO_2 in addition to the dilution effect (e.g., Gleitz et al., 1995). However in the coastal landfast ice near Barrow, high algal biomass and high productivity are concentrated into a very thin bottom layer (own data, Manes and Gradinger, 2009), while our brine sack hole sampling reflects mostly the conditions in the ice interior. The large spatial separation between the sack holes and the bottom of the sea ice (close to 1 m) and the relatively constant concentration of algae in these bottom layers makes it unlikely that the observed DIC changes over time were related to the algal activity.

A wide range of variation was evident in the replicate flux measurements on 23 May 2008 (Fig. 7). On this day, air temperature increased substantially over a short time period, compared to more stable conditions during the other dates (see Fig. 2a). While we carried out the replicate measurements within a short period (2–3 h) from morning

(9:00a.m.) to afternoon (13:00p.m.) for each sampling date, these large variations reflect the impact of rapid melting and surface warming on the CO_2 flux (Fig. 2a).

The negative CO_2 flux occurred although superimposed ice formed as a result of a rain event and snow melt (Figs. 4 and 5). The low-salinity, low- $\delta\ ^{18}O$ layer in the uppermost 3 cm of the ice core, shown for 26 May in Figs. 4 and 5, consists in fact roughly half of meteoric water (snow melt, precipitation), based on the stable oxygen isotope data. Formation of superimposed ice early in the melt season is common, and has been linked to retention of meltwater at the ice surface in the early stages of melt (Eicken et al., 2004). Our present measurements demonstrate that the superimposed ice layer does not necessarily shut down the gas exchange between the atmosphere and the upper ice layers.

The snow cover on sea ice can influence gas exchange by acting as an impermeable medium for CO_2 transfer and partially blocking CO_2 diffusion (Nomura et al., in press-a). Therefore, we cannot exclude that the absolute flux values would be higher (both for fluxes into and out of the ice) if snow were absent from the surface. Although this finding needs to be substantiated by further observations, it suggests that the progression from spring to snow-free summer conditions is in fact a very sharp transition for the carbonate system with implications for atmospheric exchange over sea ice.

Internal ice melt due to warming also contributed to the decrease of brine DIC (in addition to importing low-DIC snow meltwater into the ice cover); both processes simultaneously contributing to change sea ice from a CO_2 source to a sink for the atmosphere. Since sampling of brine from sack holes draws on a larger ice volume and may be affected by surface runoff, estimates of CO_2 fluxes based on brine CO_2 measurements alone may be associated with some errors during the transition period. However, the independent determination of the flux based on the chamber measurements substantiates the important role of brine dilution in driving the exchange of CO_2 between atmosphere and sea ice.

Much higher magnitudes in the downward-directed CO_2 flux, ranging between −38.6 and −19.5 mmol m^{-2} day^{-1} were observed over melt ponds and highly permeable ice with open brine channels in the landfast ice near Point Barrow, Alaska almost one month later in the season (4–26 June) at a time when daily mean temperatures were above 0 °C (Semiletov et al., 2004). Under these conditions, melt ponds and open brine channels can effectively exchange CO_2 because they are exposed directly to the atmosphere, similar to the free ocean surface. However, CO2 flux results over sea ice from open-path eddy covariance systems, like that used by Semelitov et al. (2004) should be interpreted with caution, given that the fluxes may be prone biases, not fully yet understood by the flux community ([Burba et al., 2008] and [Amiro 2010]).

6. Conclusions

During the rapid transition of sea ice from a “cold” early spring to a “warm” late spring state, the air–sea ice CO_2 flux decreased from +0.7 to −1.0 mmol m^{-2} day^{-1} with a corresponding rapid and highly correlated decrease in brine salinity and brine DIC. These results suggested that the sea ice shifted from a source to a sink for atmospheric CO_2, with rapid decrease of brine DIC likely associated with a decrease in brine pCO_2 from a supersaturated to an undersaturated state compared to the atmosphere. While snow deposited over sea ice and formation of superimposed ice did not completely seal off the ice interior from the atmosphere, it remains to be investigated to what extent snow and superimposed ice are impeding gas exchange, relative to higher fluxes measured over much warmer sea ice in an advanced state of melt.

This study provides valuable information on the brine biogeochemistry and gas exchange processes between the atmosphere and sea ice during the rapid cold/warm transition in landfast sea ice in the seasonally ice-covered Chukchi Sea. However, this is only a first step towards regional carbon cycle assessments in seasonally ice-covered waters, since the effect of parameters, such as snow depth, snow properties, surface

state of the sea ice, its porosity and permeability need to be investigated in more depth as well.

To our knowledge, this is the first time that such a rapid and substantial change in the air–sea ice CO_2 flux has been reported for Arctic ice-covered regions. While the onset of melt in this case was triggered by a rain event, such rapid transitions in the thermal state of the sea ice are not unusual for the Arctic (Perovich et al., 2003) and may well be typical of the marginal seas, where interaction with land surface processes impacts melt patterns.

Acknowledgements

Prof. J. L. Tison and two anonymous referees are thanked for their constructive comments that improved the paper. This study was supported by the Research Fellowship of the Japan Society for the Promotion of Science (#195968) and funds from University of Alaska Fairbanks and International Antarctic Institute (IAI) of Hokkaido University. Support by the National Science Foundation (OPP-0632398 and 0805703) is gratefully acknowledged. We express heartfelt thanks to all the members of the GEOS/MSL 695 field techniques in the interdisciplinary sea–ice research, jointly with University of Alaska Fairbanks and Hokkaido University for sampling assistance and for analyzing samples. Thanks also to Prof. H. Y. Inoue, Prof. M. Fukuchi, Prof. T. Odate, Dr. T. Toyota and Dr. S. Aoki for providing measurement devices and for their useful comments.

References

Amiro 2010 B. Amiro, Estimating annual carbon dioxide eddy fluxes using open-path analysers for cold forest sites, *Agricultural and Forest Meteorology* 150 (2010), pp. 1366–1372.

Arar and Collins, 1992 Arar, E. J., Collins, G. B., 1992. In Vitro determination of chlorophyll *a* and phaeophytin *a* in marine and freshwater phytoplankton by fluorescence. Method 445.0 Version 1.1. US EPA, Environmental Monitoring Systems Laboratory, Office of Research and Development, Cincinnati, OH.

Burba et al., 2008 G.G. Burba, D.K. McDermitt, A. Grelle, D.J. Anderson and L. Xu, Addressing the influence of instrument surface heat exchange on the measurements of CO_2 flux from open-path gas analyzers, *Global Change Biology* 14 (2008), pp. 1854–1876.

Cox and Weeks, 1983 G.F.N. Cox and W.F. Weeks, Equations for determining the gas and brine volumes in sea–ice samples, *Journal of Glaciology* 29 (1983), pp. 306–316.

Culberson et al., 1970 C. Culberson, R.M. Pytkowicz and J.E. Hawley, Seawater alkalinity determination by the pH method, *Journal of Marine Research* 28 (1970), pp. 15–21.

Delille, 2006 Delille, B., 2006. Inorganic carbon dynamics and air–ice–sea CO_2 fluxes in the open and coastal waters of the Southern Ocean. Ph.D. University of Liége, Belgium, 1–297.

Dickson and Millero, 1987 A.G. Dickson and F.J. Millero, A comparison of the equilibrium constants for the dissociation of carbonic acid in seawater media, *Deep-Sea Research* 34 (1987), pp. 1733–1743.

Dickson, 1990 A.G. Dickson, Thermodynamics of the dissociation of boric acid in synthetic seawater from 273.15 to 318.15 K, *Deep-Sea Research* 37 (1990), pp. 755–766.

DOE, 1994 DOE, 1994. Handbook of methods for the analysis of the various parameters of the carbon dioxide system in sea water, Version 2 Dickson, A.G., Goyet, C. (Eds.), ORNL/CDIAC-74, Oak Ridge National Laboratory, Oak Ridge TN.

Druckenmiller et al., 2009 M.L. Druckenmiller, H. Eicken, M.A. Johnson, D.J. Pringle and C.C. Williams, Toward an integrated coastal sea–ice observatory: system components and a case study at Barrow, Alaska, *Cold Regions Science and Technology* 56 (2009), pp. 61–72.

Eicken et al., 2004 H. Eicken, T.C. Grenfell, D.K. Perovich, J.A. Richter-Menge and K. Frey, Hydraulic controls of summer Arctic pack ice albedo, *Journal of Geophysical Research* 109 (2004), p. C08007 10.1029/2003JC001989.

Frankignoulle, 1998 M. Frankignoulle, Field measurements of air–sea CO_2 exchange, *Limnology and Oceanography* 33 (3) (1998), pp. 313–322.

Gleitz et al., 1995 M. Gleitz, M.R. Vonderlo, D.N. Tomas, G.S. Dieckmann and F.J. Millero, Comparison of summer and winter inorganic carbon, oxygen and nutrient concentrations in Antarctic sea ice brine, *Marine Chemistry* 51 (1995), pp. 81–89.

Golden et al., 1998 K.M. Golden, S.F. Ackley and V.I. Lytle, The percolation phase transition in sea ice, *Science* 282 (1998), pp. 2238–2241.

Inoue and Ishii, 2005 H.Y. Inoue and M. Ishii, Variations and trends of CO_2 in the surface seawater in the Southern Ocean south of Australia between 1969 and 2002, *Tellus* 57B (2005), pp. 58–69.

Johnson et al., 1985 K.M. Johnson, A.E. King and J.M. Sieburth, Coulometric TCO_2 analyses for marine studies: an introduction, *Marine Chemistry* 16 (1985), pp. 61–82.

Leppäranta and Manninen, 1988 M. Leppäranta and T. Manninen, The brine and gas content of sea ice with attention to low salinities and high temperatures, *Finnish Institute of Marine Research Internal Report* 88-2 (1988) Helsinki.

Lewis and Wallace, 1998 E. Lewis and D.W.R. Wallace, Program Developed for CO_2 System Calculations. ORNL/CDIAC-105, Carbon Dioxide Information Analysis Center, Oak Ridge National Laboratory, U.S. Department of Energy, Oak Ridge, Tennessee (1998).

Loose et al., 2009 B. Loose, W.R. McGillis, P. Schlosser, D. Perovich and T. Takahashi, Effects of freezing, growth, and ice cover on gas transport processes in laboratory seawater experiments, *Geophysical Research Letters* (2009), p. 36 10.1029/2008GL036318.

Luo and Zhou, 2006 Y. Luo and X. Zhou, Methods of measurements and estimations. In: Y. Luo and X. Zhou, Editors, *Soil Respiration and the Environment*, Elsevier Inc. (2006), pp. 161–185.

Mahoney et al., 2007 A. Mahoney, H. Eicken, A.G. Gaylord and L. Shapiro, Alaska landfast sea ice: links with bathymetry and atmospheric circulation, *Journal of Geophysical Research* (2007), p. 112 10.1029/2006JC003559.

Manes and Gradinger, 2009 S. Manes and R. Gradinger, Small scale vertical gradients of Arctic ice algal photophysiological properties, *Photosynthesis Research* (2009) 10.1007/s11120-009-9489-0.

Mariko et al., 1994 S. Mariko, Y. Bekku and H. Koizumi, Efflux of carbon dioxide from snow-covered forest floors, *Ecological Research* 9 (1994), pp. 343–350.

Mehrbach et al., 1973 C. Mehrbach, C.H. Culberson, J.E. Hawley and R.M. Pytkowicz, Measurement of the apparent dissociation constant of carbonic acid in seawater at atmospheric pressure, *Limnology and Oceanography* 18 (1973), pp. 897–907.

Millero, 1995 F.J. Millero, Thermodynamic of the carbon dioxide system in the oceans, *Geochimca et Cosmochimica Acta* 59 (1995), pp. 661–677.

Nomura et al., 2006 D. Nomura, Y.H. Inoue and T. Toyota, The effect of sea ice growth on air–sea CO_2 flux in a tank experiment, *Tellus* 58B (2006), pp. 418–426.

Nomura et al., 2009 D. Nomura, T. Takatsuka, M. Ishikawa, T. Kawamura, K. Shirasawa and Y.H. Inoue, Transport of chemical components in sea ice and under-ice water during melting in the seasonally ice-covered Saroma-ko Lagoon, Hokkaido, Japan, *Estuarine, Coastal and Shelf Science* 81 (2009), pp. 201–209.

Nomura et al., in press-a Nomura, D., Inoue, Y. H., Toyota, T., Shirasawa, K., in press-a. Effects of snow, snow-melting and re-freezing on air–sea ice CO_2 flux. Journal of Glaciology.

Nomura et al., in press-b Nomura, D., Nishioka, J., Granskog, M. A., Krell, A., Matoba, S., Toyota, T., Hattori, H., Shirasawa, K., in press-b. Nutrient distributions associated with snow and sediment-laden layers in sea ice of the southern Sea of Okhotsk. Marine Chemistry.

Papadimitriou et al., 2003 S. Papadimitriou, H. Kennedy, G. Kattner, G.S. Dieckmann and D.N. Thomas, Experimental evidence for carbonate precipitation and CO_2 degassing during sea ice formation, *Geochimica et Cosmochimica Acta* 68 (2003), pp. 1749–1761.

Perovich et al., 2003 D.K. Perovich, T.C. Grenfell, J.A. Richter-Menge, B. Light, W.B. Tucker III and H. Eicken, Thin and thinner: sea ice mass balance measurements during SHEBA, *Journal of Geophysical Research* 108 (C3) (2003), p. 8050 10.1029/2001JC001079.

Pipko et al., 2002 I.I. Pipko, I.P. Semiletov, P.Y. Tishchenko, S.P. Pugach and J.P. Christensen, Carbonate chemistry dynamics in Bering Strait and the Chukchi Sea, *Progress in Oceanography* 55 (2002), pp. 77–94.

Rysgaard et al., 2007 S. Rysgaard, R.N. Glud, M.K. Sejr, B. Bendtsen and P.B. Christensen, Inorganic carbon transport during sea ice growth and decay: a carbon pump in polar seas, *Journal of Geophysical Research* 112 (2007), p. C03016 10.1029/2006JC003572.

Schindlbacher et al., 2007 A. Schindlbacher, S. Zechmeister-Boltenstern, G. Glatzel and R. Jandl, Winter soil respiration from an Austrian mountain forest, *Agricultural and Forest Meteorology* 146 (2007), pp. 205–215.

Semiletov et al., 2004 I.P. Semiletov, A. Makshtas, S. Akasofu and E. Andreas, Atmospheric CO_2 balance: the role of Arctic sea ice, *Geophysical Research Letters* (2004), p. 31 10.1029/2003GL017996.

Semiletov et al., 2007 I.P. Semiletov, I.I. Pipko, I. Repina and N.E. Shakhova, Carbonate chemistry dynamics and carbon dioxide fluxes across the atmosphere–ice–water interfaces in the arctic ocean: pacific sector of the arctic, *Journal of Marine Systems* 66 (2007), pp. 204–226.

Takagi et al., 2005 K. Takagi, M. Nomura, D. Ashiya, H. Takahashi, K. Sasa, Y. Fujinuma, H. Shibata, Y. Akibayashi and T. Koike, Dynamic carbon dioxide exchange through snowpack by wind-driven mass transfer in a conifer-broadleaf mixed forest in northernmost Japan, *Global Biogeochemical Cycles* 19 (2005), p. GB2012 10.1029/2004GB002272.

Takahashi et al., 2009 T. Takahashi, S.C. Sutherland, R. Wanninkhof, C. Sweeney, R.A. Feely, D.W. Chipman, B. Hales, G. Friederich, F. Chavez, C. Sabine, A. Watson, D.C.E. Bakker, U. Schuster, N. Metzl, H. Yoshikawa-Inoue, M. Ishii, T. Midorikawa, Y. Nojiri, A. Körtzinger, T. Steinhoff, M. Hoppema, J. Olafsson, T.S. Arnarson, B. Tilbrook, T. Johannessen, A. Olsen, R. Bellerby, C.S. Wong, B. Delille, N.R. Bates, H.J. Baar and W. de, Climatological mean and decadal change in surface ocean pCO_2, and net sea–air CO_2 flux over the global oceans, *Deep-Sea Research II* 56 (2009), pp. 554–577.

Thomas et al., 2010 D.N. Thomas, S. Papadimitriou and C. Michel, Biogeochemistry of sea ice. In: D.N. Thomas and G.S. Dieckmann, Editors, *Sea ice* (second edn.), Wiley-Blackwell, Oxford (2010), pp. 425–467.

Tison et al., 2002 J.L. Tison, C. Haas, M.M. Gowing, S. Sleewaegen and A. Bernard, Tank study of physico-chemical controls on gas content and composition during growth of young sea ice, *Journal of Glaciology* 48 (161) (2002), pp. 177–191.

Wakita et al., 2005 M. Wakita, S. Watanabe, Y.W. Watanabe, T. Ono, N. Tsurushima and S. Tsunogai, Temporal change of dissolved inorganic carbon in the subsurface water at station KNOT (44°N, 155°N) in the western North Pacific subpolar region, *Journal of Oceanography* 61 (2005), pp. 129–139.

Weiss and Price, 1980 R.F. Weiss and B.A. Price, Nitrous oxide solubility in water and seawater, *Marine Chemistry* 8 (1980), pp. 347–359.

Winston et al., 1995 Winston, G. C., Stephens, B. B., Sundquest, E. T., Hardy J. P., Davis, R. E., 1995. Seasonal variability in CO_2 transport through snow in a boreal forest. Biogeochemistry of seasonally snow-covered catchments. In: Proceedings of a Boulder Symposium, July 1995. IAHS Publ. 228, 61–70.

Zemmelink et al., 2006 H.J. Zemmelink, B. Delille, J.L. Tison, E.J. Hintsa, L. Houghton and J.W.H. Dacey, CO_2 deposition over the multi-year ice of the western Weddell Sea, *Geophysical Research Letters* (2006), p. 33 10.1029/2006GL026320.

Figure captions

Fig. 1.
Location map of the sampling site on first-year landfast sea ice in the Chukchi Sea, off Barrow, Alaska.

Fig. 2.
Temporal variations of (a) air and (b) sea ice temperatures at the Barrow sea ice mass balance site.

Fig. 3.
Temporal variations of (a) sea ice thickness and (b) snow depth at the sampling station. Snow depth was measured at the chamber setting site.

Fig. 4.
(a) $\delta^{18}O$ profile through snow and upper sea ice layers at the ice sampling site on 26 May 2008 and (b) shown at right at the same scale as the depth axis, is the core stratigraphy from a photograph taken at the sampling site.

Fig. 5.
Vertical profiles of (a) bulk ice salinity, (b) ice temperature, (c) brine volume and (d) chlorophyll *a* concentration at the sampling station for each day. “ND” indicates no data.

Fig. 6.
Temporal variations of (a) temperature, (b) salinity and (c) DIC of brine and under-ice water and (d) salinity normalized-brine DIC at the sampling station. Solid gray line in (d) indicates the best fit to describe the relationship.

Fig. 7.
Temporal variations of air–sea ice CO_2 flux at the sampling station. Open square indicates the value obtained from a single measurement. Open circle with error bar indicates the mean value obtained from duplicate measurements within 2–3 h at the same area. Error bar indicates the maximum and minimum values of duplicate measurements.

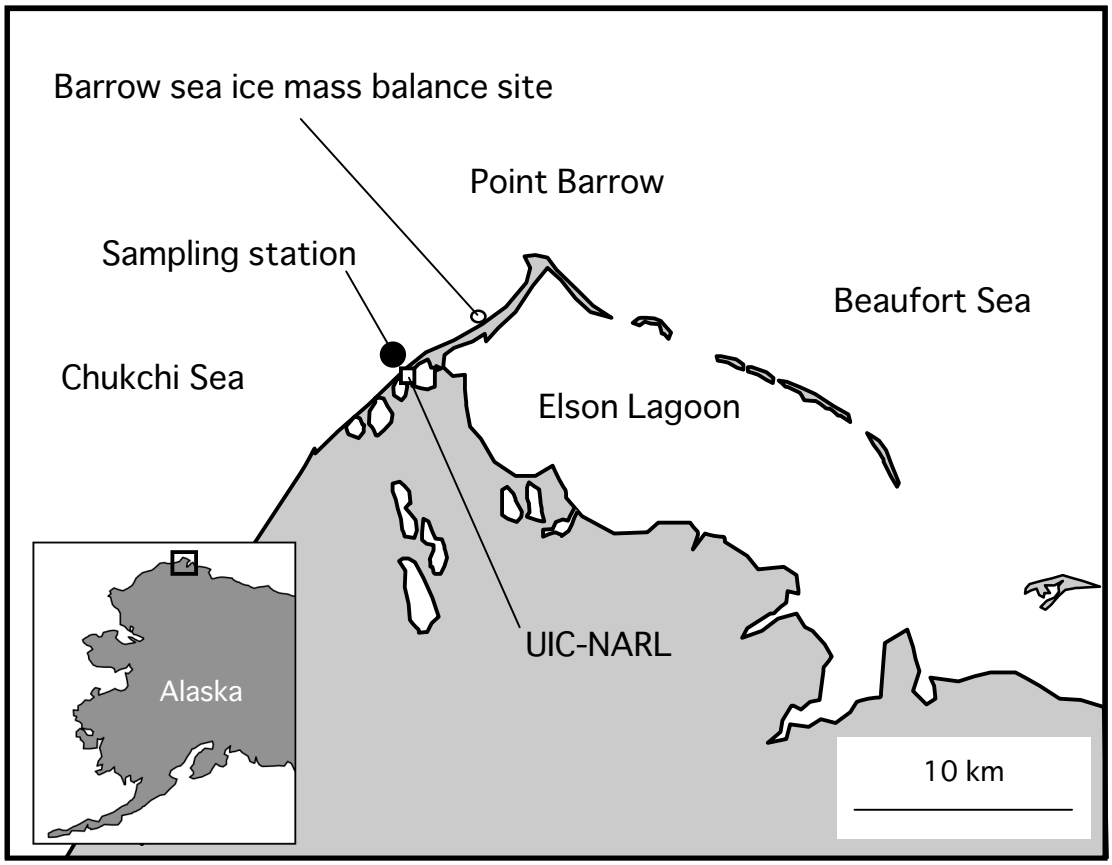

Figure 1, Nomura et al.

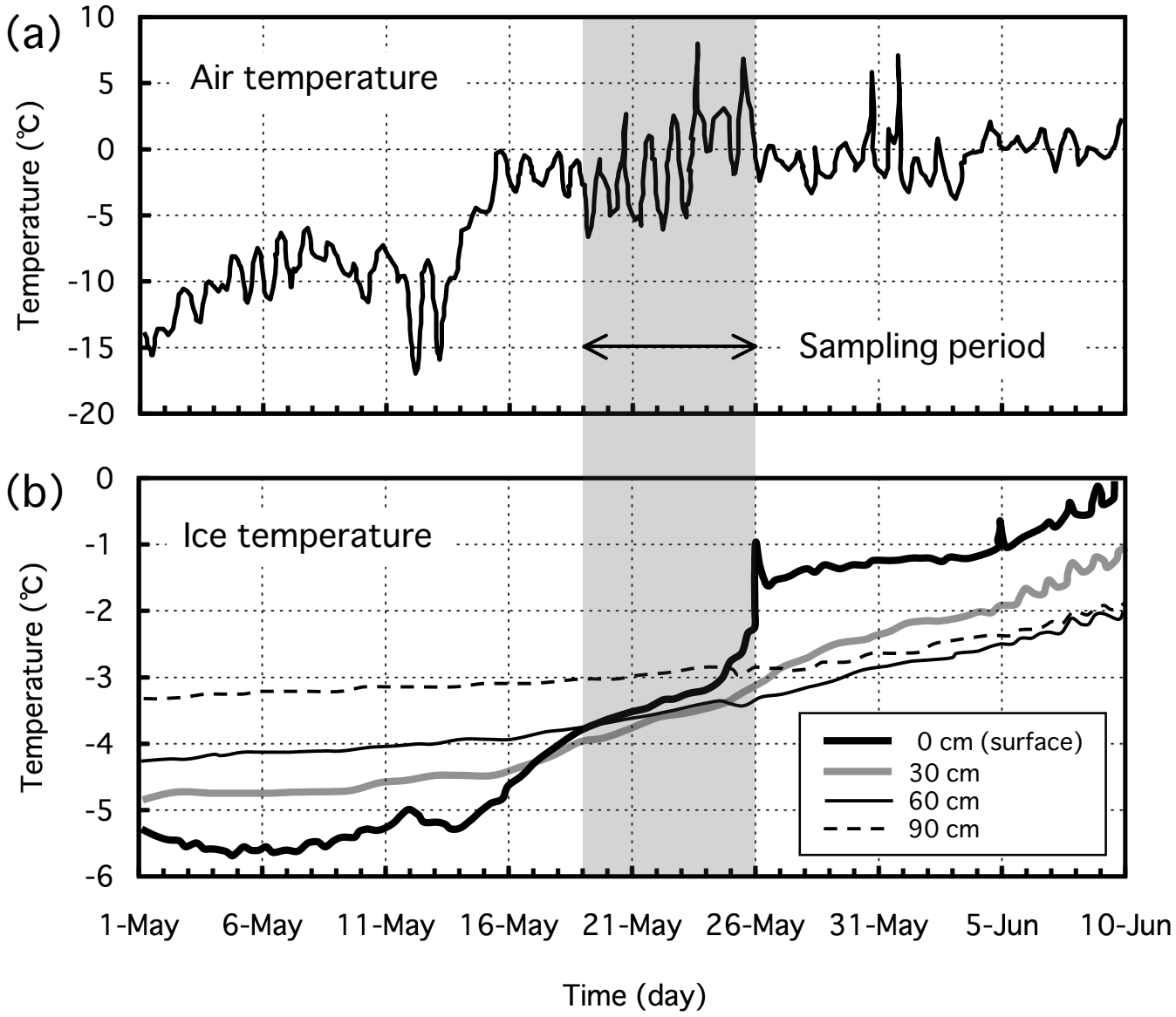

Figure 2, Nomura et al.

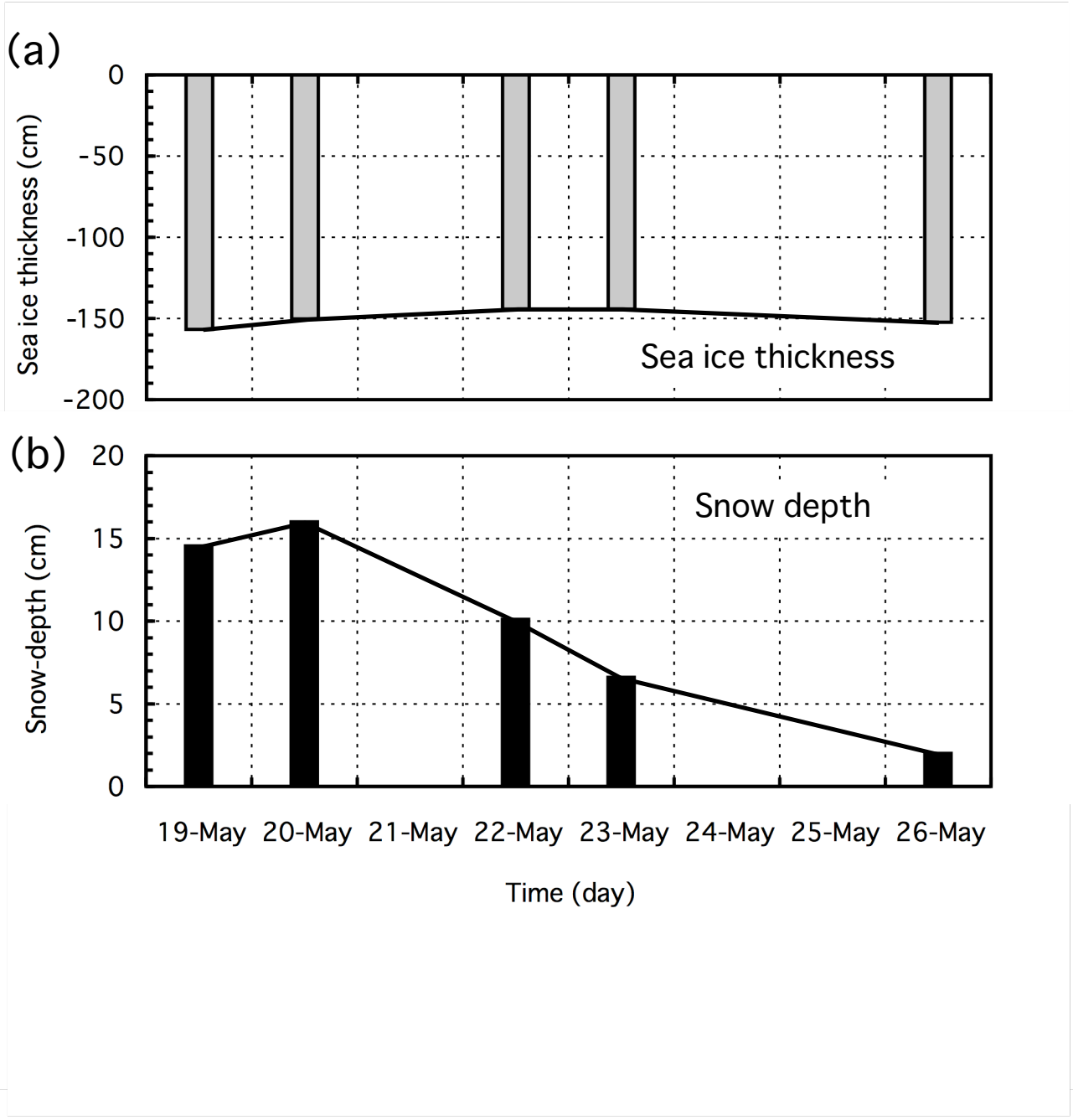

Figure 3, Nomura et al.

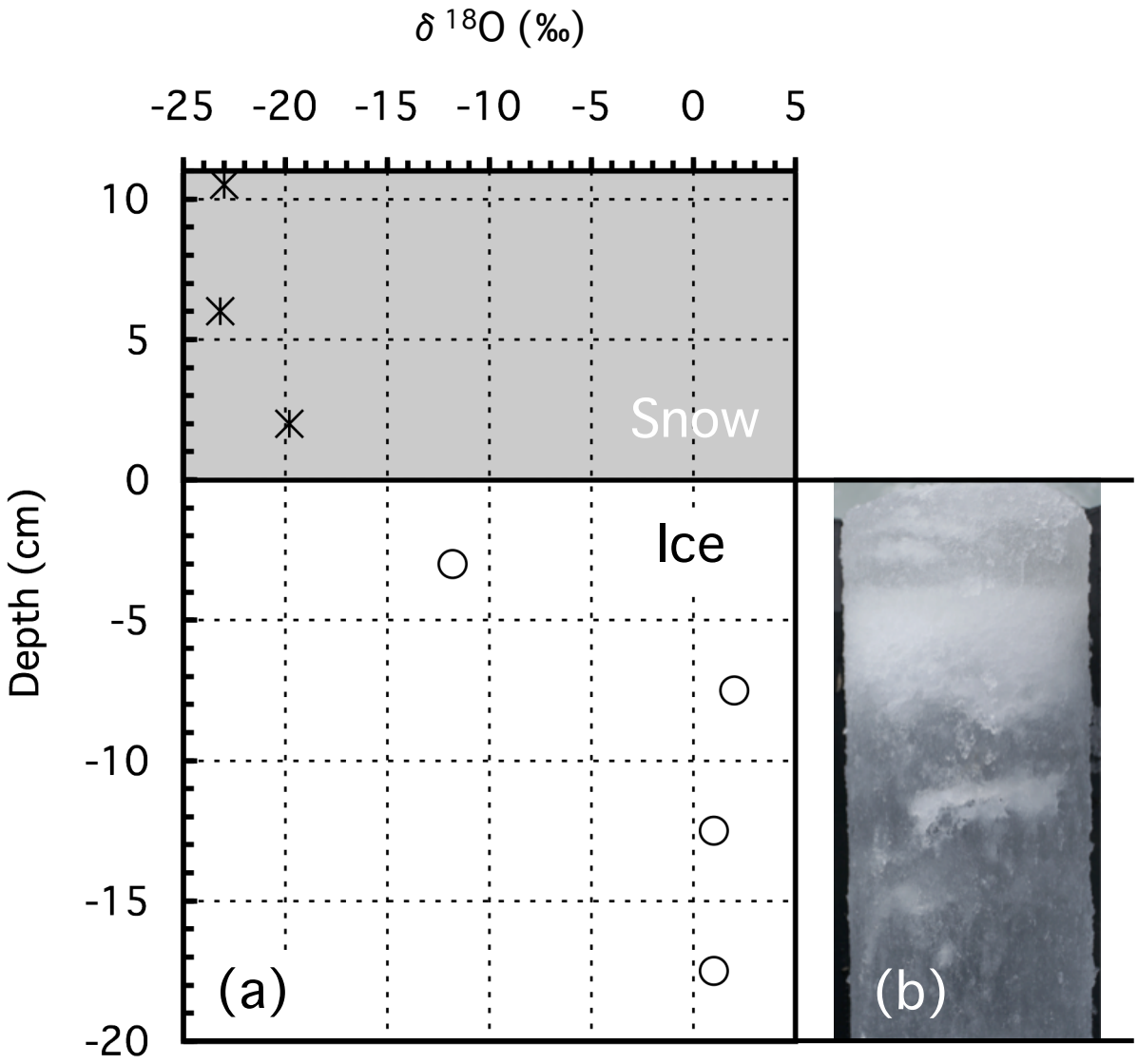

Figure 4, Nomura et al.

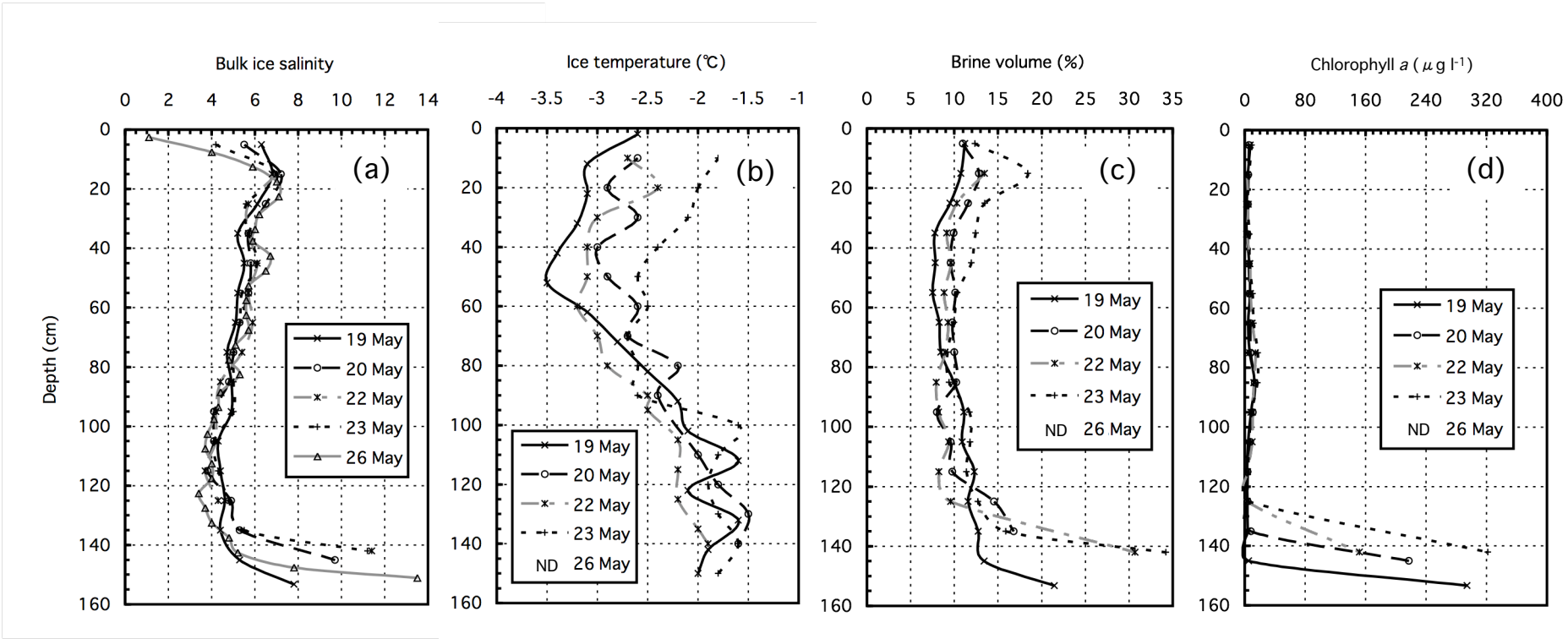

Figure 5, Nomura et al.

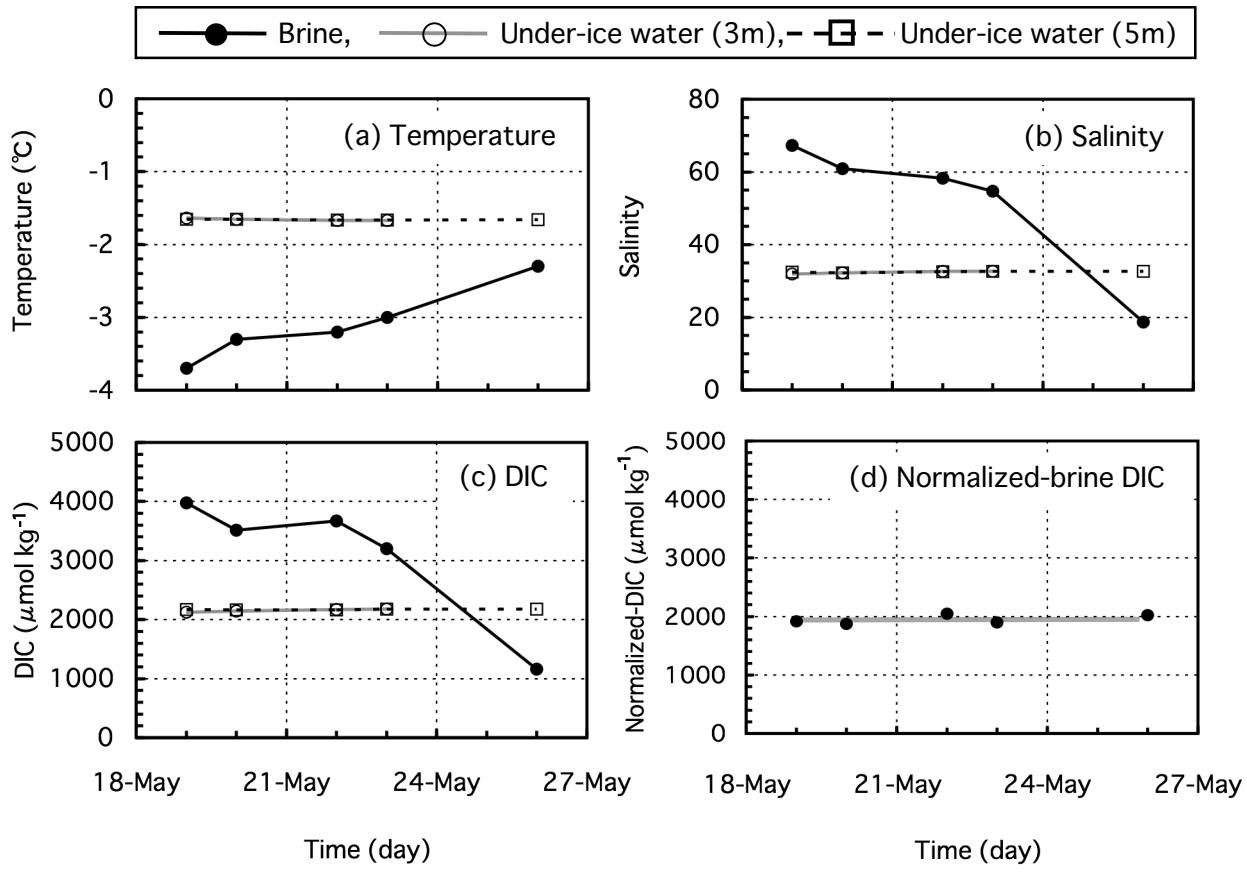

Figure 6, Nomura et al.

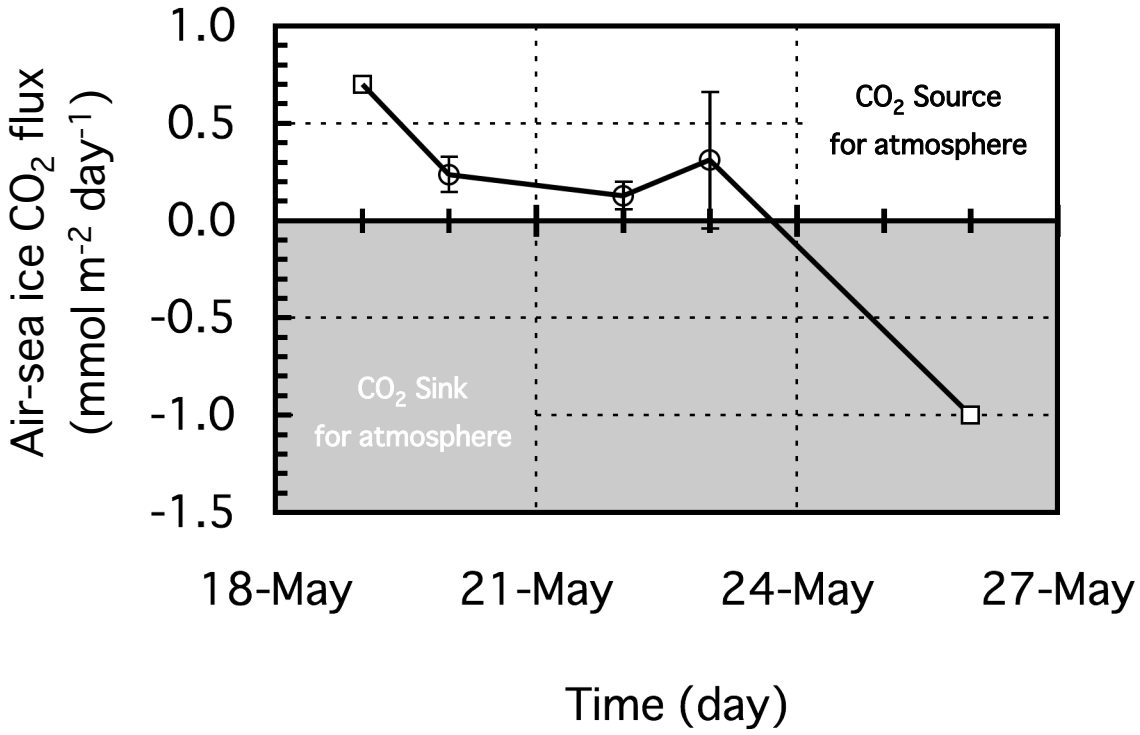

Figure 7, Nomura et al.